Chapter 3

TDR-Based Identification Approach

3.1 Introduction

This chapter takes the previous chapter's study of bounce diagrams and the TDR response a step further and presents a TP loop identification approach using the TDR response for its available measurements. An iterative procedure is proposed to exploit the information embedded in the individual reflections of the TDR response. The three elements of the approach addressed in this chapter are:

- Iterative loop structure modeling (Section 3.2).
- Detection of the first unresolved reflection (Section 3.3).
- Estimation of the loop parameters from the selected reflection (Section 3.4).

Each reflection is returned from a particular node in the loop and possesses sufficient characteristics to determine the node parameters — the length of the leading segment and the node and TP types. One reflection is processed per iteration; each revealing a new node of the subscriber loop. In order to process a TDR reflection, the reflection first needs to be detected on the basis of weighted cumulative squared error (WCSSE). Subsequently, with respect to the detected reflection, the loop parameters related to the loop node are estimated.

This proposed algorithm is found susceptible to heavily overlapped reflections. Section 3.5 discusses this issue and demonstrates it through the CSA #1 test loop identification from Node 1.

3.2 Iterative Loop Structure Modeling

In Chapter 2 the TP loop environment for TDR responses was discussed, with a behavior often illustrated by bounce diagrams. The latter suggested that the TDR response is a sum of reflected pulses

from all of the loop nodes. The TDR response analysis also provided the intuition that there are considerable delays between reflections if the separation between nodes is sufficiently large compared to the TDR input pulse width, and that the structure of the loop beyond a node does not influence its initial reflection at all.

Consequently, analyzing a reflection can uncover a new loop node and its parameters. The node parameters include the node distance (both in the temporal and the spatial sense) from the measurement node and the number and types of TP lines connected to the node. The temporal node location corresponds to the time-of-arrival (TOA) of the initial reflection from the node, while the spatial location relates to a specific location on the loop structure graph. Note that multiple equivalent spatial locations may exist for a temporal node location. Identifying the spatial location of the new node yields a length estimate for the leading TP segment (*i.e.*, the segment that connects the new node to one of the known nodes).

One approach to loop structure identification is to process all reflections simultaneously to reveal the responsible loop nodes and gather all findings to construct a loop model in a single step. However, this approach is only feasible for a distortionless transmission line network, in which all TDR reflections possess the exact shape of the input pulse and in which the source impedance perfectly matches that of the connected line. The TP loop, as discussed in Section 2.4, does not fall in this class of transmission lines and is observed to be dispersive. The dispersive type of transmission medium causes TDR reflections to possess a "tail" (see Figure 2-14). Consequently, the reflection tail overlaps with and obscures subsequent reflections, making the possibility of simultaneous loop node identification extremely challenging.

To overcome the overlapping problem, an iterative modeling procedure is proposed. Starting with a measurement node alone, this approach takes one reflection at a time and expands the partially constructed model with an additional node to account for the reflection. This facilitates the removal of previously identified reflections by subtracting the simulated TDR response of the partial model from the measurement. The partial model includes all of the identified nodes. Another advantage gained with this method is that the simulated TDR response of the partial model also includes the secondary reflections from a node caused by the impedance mismatching at the source node. The iteration termination condition occurs when no segments in the loop model are infinitely long. This condition therefore implies that the partial model can no longer accept new nodes.

While the partial model needs to encompass all of the identified reflections, it is equally important not to disturb the remaining reflections (*i.e.*, the partial loop should not introduce superfluous

reflections not supported by the measurements). This is achieved by modeling the TP segment of unknown length as infinitely long. Signals traveling on an infinitely long line never return, and as a result the partial loop only takes into account what is already known.

This modeling technique can be readily verified with the block diagram representation of the TDR system with the single segment LUI in Figure 2-11. Suppose that the measurement node (Node 1) is properly identified and the identified segment is modeled as infinitely long as shown in Figure 3-1. This suggests that the TP type of the first segment is determined. The identification of the first node is achieved by processing the first reflection, traveled on the red path shown in Figure 3-2. The remaining unresolved paths are the initial reflection path from the far end (in blue) and its secondary reflection path (in green). The partial model in Figure 3-1 only models the red path, without any additional reflections. Moreover, $\Gamma_{11}(f)$, $T_{11}(f)$, and $\gamma_1(f)$ have already been determined by the first reflection, leaving the segment length l_1 as the only variable. Therefore, to remove the unwanted paths, l_1 is set equal to infinity, which effectively forces the $e^{-\gamma_1(f)l_1}$ block to be zero.

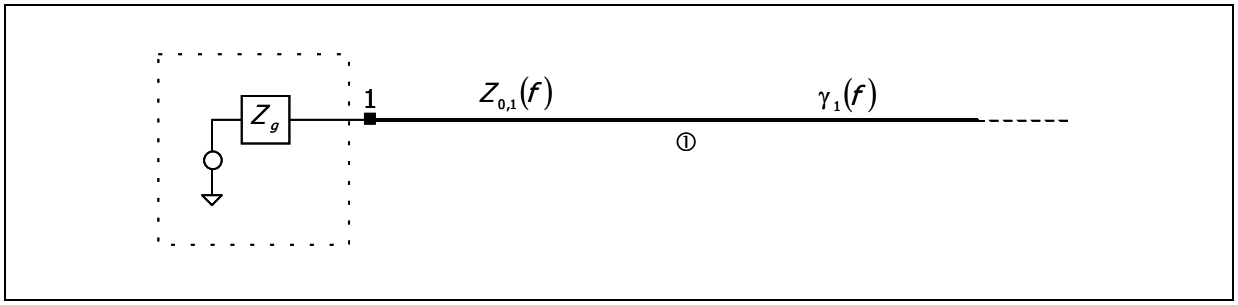

Figure 3-1: Partial loop model after first iteration.

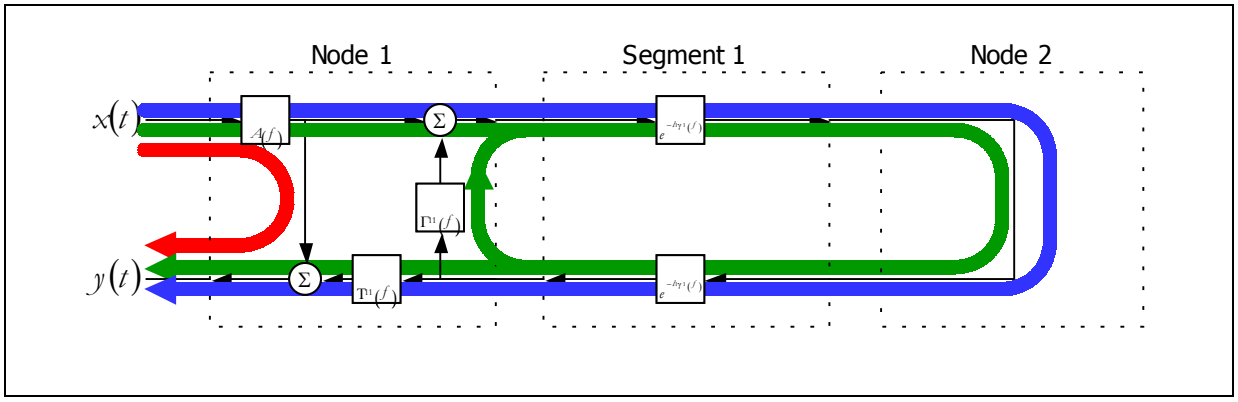

Figure 3-2: Illustration of initial reflection (red), Node 2 first reflection (blue), and Node 2 secondary reflection (green) paths for the loop in Figure 2-11.

Furthermore, the overall TDR response and the partial model TDR response are shown in Figure 3-3. Note that the model response is identical to that in Figure 2-14(a) which is the first reflection in the TDR response. The point where the deviation between the LUI and partial model responses occurs corresponds to the beginning of the second reflection, which relates to Node 2. The Node 2 initial reflection (blue path) determines the loop segment length and the node type as termination. After proper identification of Node 2, the remaining secondary reflections (green path) can be modeled with the complete loop model.

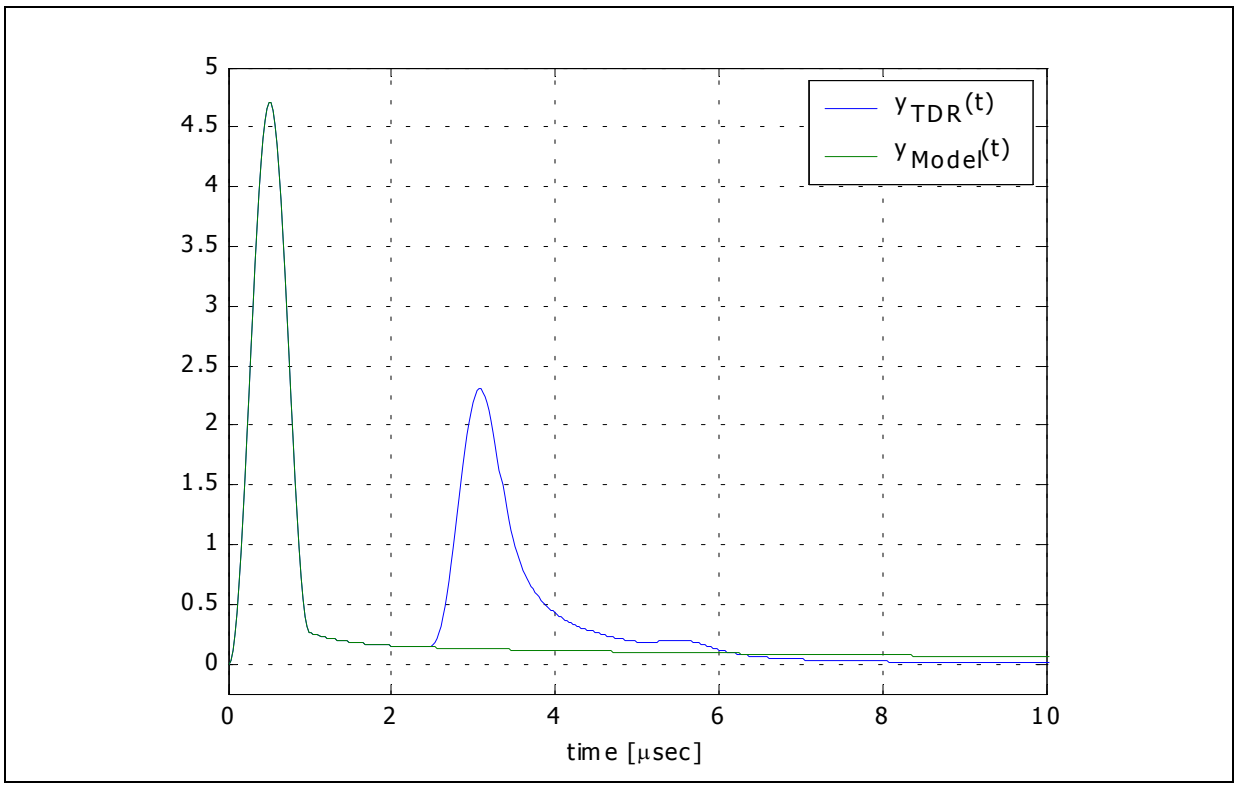

Figure 3-3: TDR response and partial model with infinitely long segment.

3.3 TDR Reflection Detection

Each iteration of the iterative modeling procedure begins with the detection of a reflection, indicating where the next unresolved reflection is (approximately) located. With human perception, this is a relatively simple task — compare the response and the model, and estimate a time when the two start to deviate. However, this perceptually simple task is challenging for a computer algorithm. The approach that we have adopted is based on the weighted cumulative sum of squared error (WCSSE) function, which is a monotonically increasing function of time.

The deviation (e_n) between the measured and modeled TDR responses is referred to as a residual or error,

$$e_n = y_{TDR,i} - \hat{y}_{TDR,i} \tag{3-1}$$

where $y_{TDR,n}$ and $\hat{y}_{TDR,n}$ are the TDR response of the LUI and the partial model, respectively, sampled at f_s (in Hertz). For example, Figure 3-4 shows the residual TDR response sampled at 40 MHz. The first of the remaining reflections clearly starts around $n = 100$ or 2.5 μs.

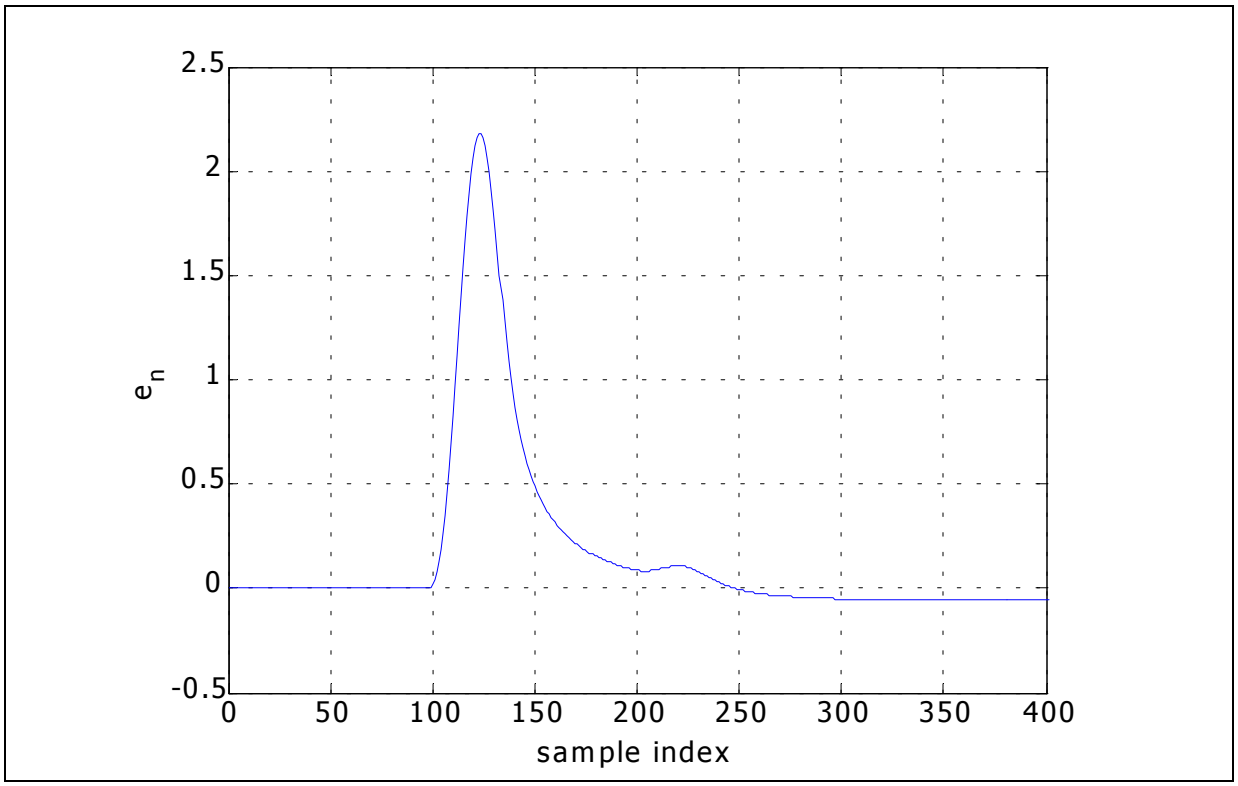

Figure 3-4: Error between the TDR responses in Figure 3-3, sampled at 40 MHz.

Under ideal circumstances, there is zero deviation between the measurement and the model over the region already processed. Consequently, the next reflection is located where the residual is no longer zero. Such an ideal condition would never arise in a practical situation, due to the introduction of noise and mismatches between the TP model and the actual TP characteristics. Instead, the cumulative sum of squared error (CSSE) function is computed to determine where the change starts to occur. The CSSE is defined as

$$CSSE_n = \sum_{i=0}^{n} e_i^2 \quad \text{for } n = 0 : N-1 . \tag{3-2}$$

where N is the number of TDR samples. The CSSE based on the error function in Figure 3-4 is shown in Figure 3-5. The function is monotonically increasing and saturates after approximately n = 200. The saturation is due to the lack of reflections that are as strong as the initial reflection, and occurs with all TP loops due to their dispersive nature. Utilizing the CSSE saturation characteristics, the time-of-arrival (TOA) of the next reflection, n_r, is estimated by

$$n_r = \arg\min_n \left(CSSE_n > \eta_r CSSE_{N-1} \right) \tag{3-3}$$

using the *ad hoc* threshold level η_r. The threshold level needs to be sufficiently small to capture the beginning of the deviation; on the other hand, the threshold must be large enough to neglect noise. We have selected $\eta_r = 0.001$ for our experiment. For the CSSE shown in Figure 3-5, $n_r = 105$, which is a good approximate result.

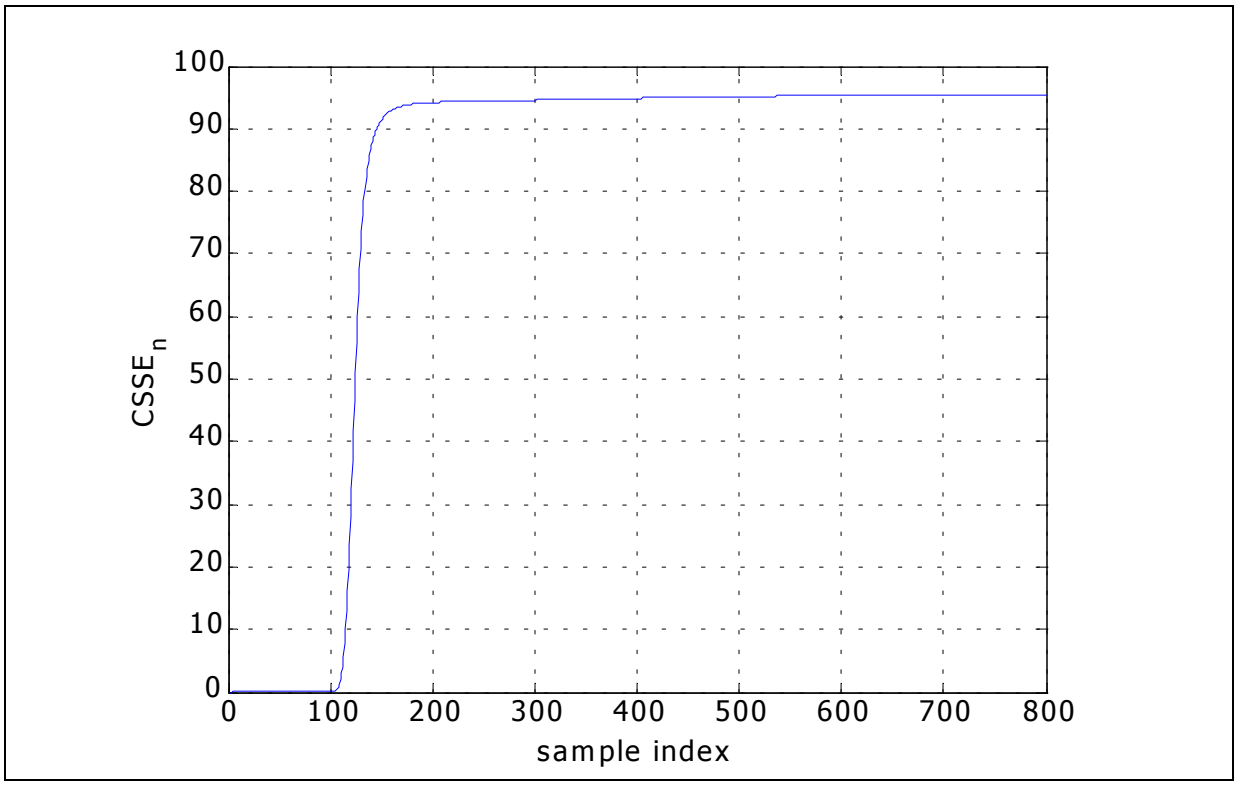

Figure 3-5: CSSE of the TDR responses in Figure 3-3.

However, the CSSE criterion assumption that the next reflection is the only strong reflection does not always hold true. A prime example of where it fails is the two-segment loop with a GC in Figure 2-15 and its TDR response in Figure 3-6(a). Again, consider the second identification iteration after the resolution of the first reflection (the model shown in Figure 3-6(b)). The CSSE at this stage is plotted in Figure 3-7. In this case, $n_r = 83$, which is overestimated by more than 20 (the true reflection TOA is about $n_r = 60$).

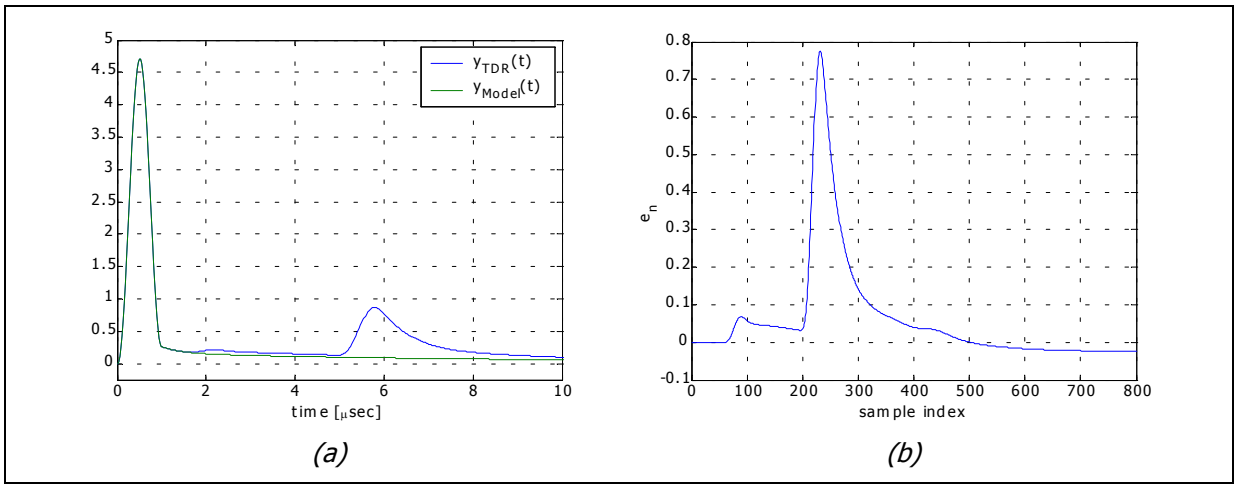

Figure 3-6: Actual and first iteration model TDR responses (a) and corresponding error (b).

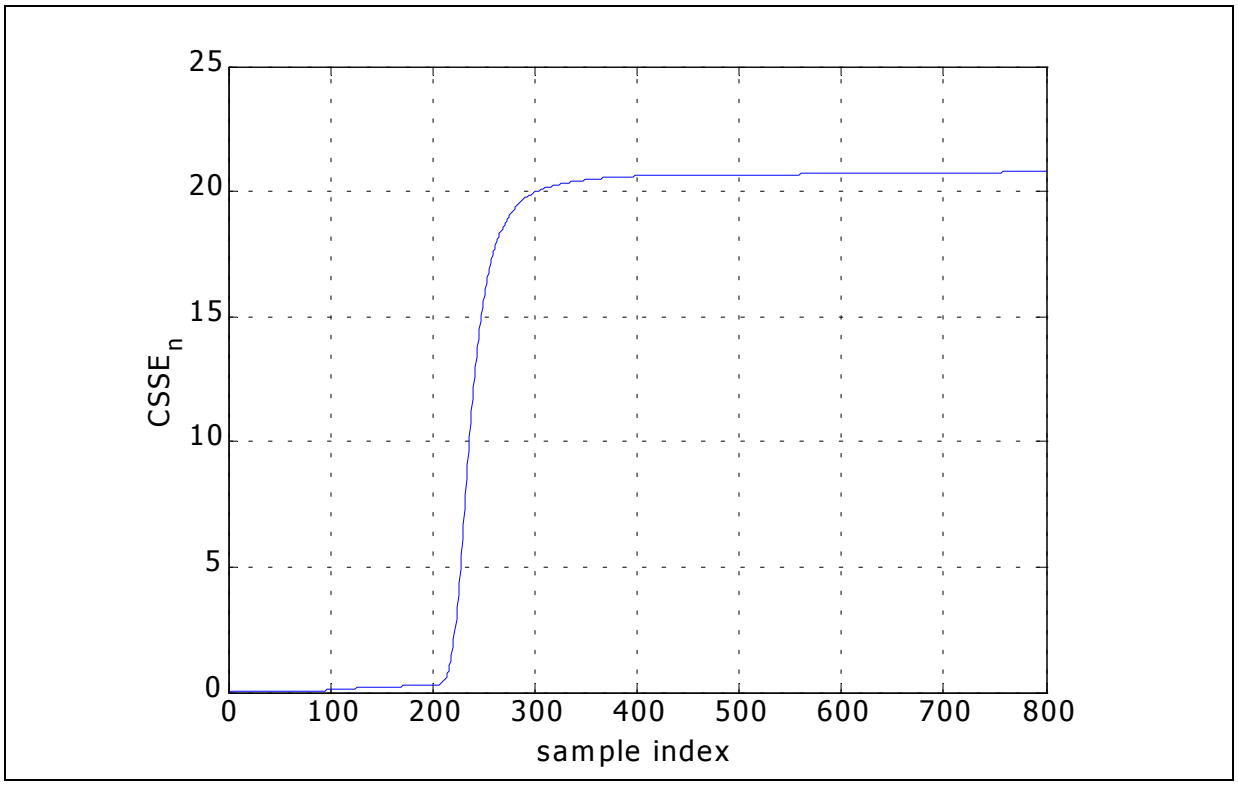

Figure 3-7: The CSSE based on the residual in Figure 3-6(b).

To compensate for this potential problem, when multiple strong reflections occur, we have explored a variation of the CSSE where a weighting function, w_n, is considered. The purpose of the weighting function is to de-emphasize the effects from later reflections. The weighted CSSE (WCSSE) is expressed as

$$WCSSE_n = \sum_{i=0}^{n} w_i e_i^2 \quad \text{for } n = 0 : N-1. \tag{3-4}$$

The weighting function that we have used is

$$w_n = \begin{cases} \dfrac{1}{(n-M)^2}, & n > M \\ 0, & otherwise \end{cases} \tag{3-5}$$

where M is a sample index corresponding approximately to the previous reflection's TOA. This offset is added to ignore errors caused by the model (mostly length estimation error) prior to the previous

reflection. For the last example where M is zero (the TOA of the first reflection is always zero), the associated WCSSE is shown in Figure 3-8, and leads to $n_r = 74$. While it is still far (approximately by 15 samples) from the actual TOA, the WCSSE estimate is closer to the actual than the CSSE counterpart.

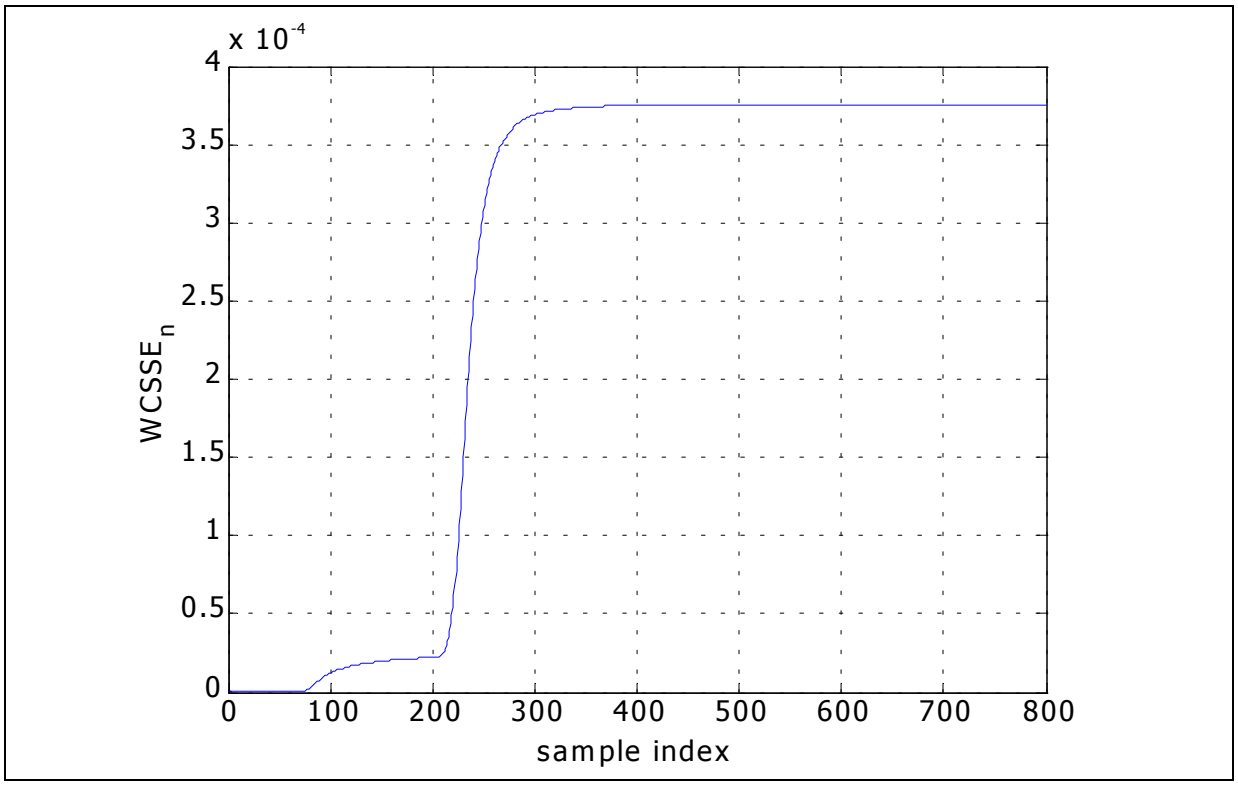

Figure 3-8: The WCSSE of residue plot in Figure 3-6(b).

The weighting function, which is selected arbitrarily, does not do a particularly good job in refining the CSSE result and produces at best a minor improvement in the reflection TOA estimate. Nonetheless, when compared to the CSSE plot, the WCSSE plot clearly illustrates the effect of the weighting function. The first raise that is associated with the reflection of interest is more apparent in the WCSSE plot than in the CSSE plot.

3.4 Loop Parameter Estimation

Once the next reflection is detected, the loop node of the LUI associated with the reflection-under-investigation (RUI) is determined (this node is referred to hereafter as the new reflection node). There are three tasks involved:

- Candidate loop model generation;
- Length refinement for each candidate model;
- Selection of the best candidate.

The length refinement procedure is applied for each individual candidate model to improve its fit. This aids the accuracy of the proceeding candidate selection process. The candidates are generated based on possible locations for the new reflection node (and can be placed on any of the existing infinitely long segments) and on the node and its TP types.

3.4.1 Initial Length Estimation

The first step in the analysis of a reflection pulse is to determine where the reflection node is on the current partial loop model (the model at the beginning of the iteration). Since the TDR reflections are processed in order of arrival, a new reflection node is assured to be located on one of the infinitely long segments of the partial loop. Recall that the partial models are modeled with infinitely long segments to avoid introducing superfluous reflections. To generate candidate models, one of the infinitely long segments is replaced with a segment that connects the new node to the segment's base node. The length of the new segment is estimated based on the TOA of the RUI.

The segment length estimate $\hat{l}$ is directly proportional to the time lag, between the TOAs of the RUI and the reflection associated with the base node of the infinitely long segment, as follows

$$\hat{l} = \frac{1}{2}\frac{n_r - n_b}{f_s}\max_{f<f_c}\left[u_g(f)\right] \tag{3-6}$$

where n_b is the TOA of the reflection associated with the base node, and $u_g(f)$ is the signal group velocity in the TP. The group velocity is defined by

$$u_g(f) = \frac{2\pi\Delta f}{\Delta\beta} = \frac{2\pi}{\partial\beta/\partial f}. \tag{3-7}$$

The velocity profiles (how the group velocity changes with respect to frequency) for the ANSI TPs under our consideration are shown in Figure 3-9. The highest group velocity within the frequency range where the reflection has substantial energy is tied with the TOA. Since the spectra of the TDR

input pulse and reflections are dominantly lowpass as shown in Figure 3-10, the highest velocity below the pulse cutoff frequency f_c is utilized in (3-6).

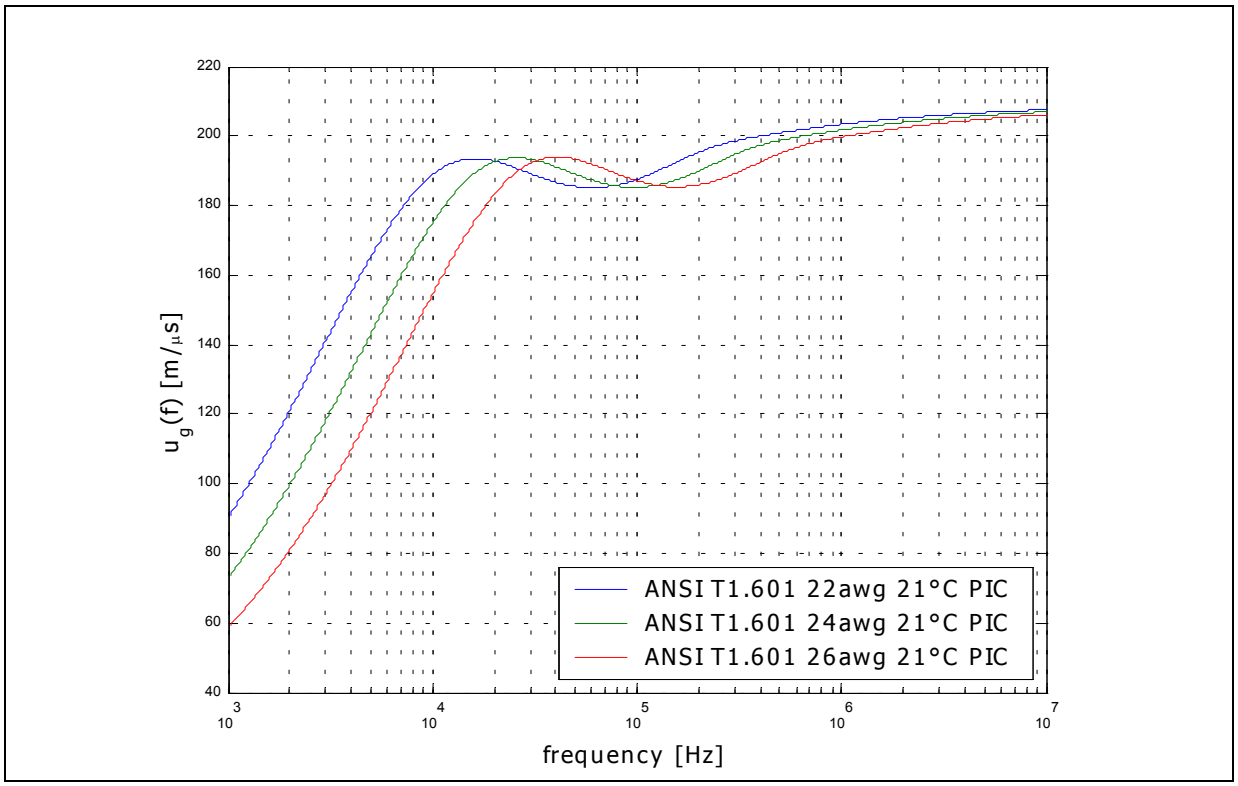

Figure 3-9: Velocity profile of the ANSI T1.601 PIC TP.

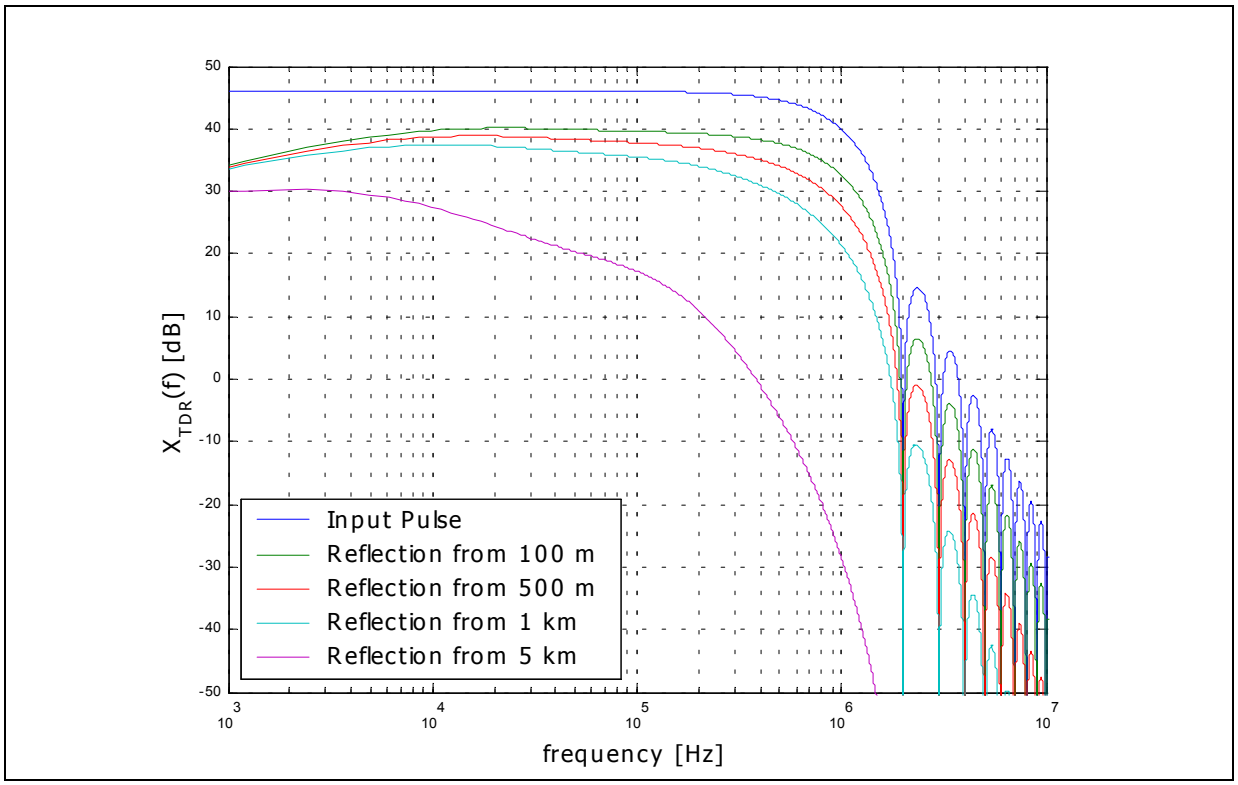

Figure 3-10: Magnitude spectrum of TDR input pulse and various reflections (single segment case).

The problem with (3-6) is that we do not know the magnitude spectrum of the RUI. However, Figure 3-10 indicates that f_c always lies in the 10 kHz to 500 kHz regions; and consequently, based on Figure 3-9, the highest velocity would be in between 180 and 200 m/μsec for all foreseeable cases (< 5km). Therefore, $\max_{f<f_c}\left|u_g(f)\right|$ is approximated by $\hat{u}_g = 190$ m/μsec. This approximation yields

$$\hat{l} = \frac{1}{2}\frac{n_r - n_b}{f_s}\hat{u}_g \tag{3-8}$$

Note that this approximation is only valid for the three TP types that we are considering. For any other TP type, a similar study is needed.

To illustrate the conversion process, the length estimate in (3-8) for the previous single segment example, where $n_r = 105$ and $n_b = 0$, yields 249.375 m. This estimate is only 0.625 m off from the actual value of 250 m. Similarly, for the gauge change example where $n_r = 74$ and $n_b = 0$, the length estimate is 175.75 m. The actual length is 150 m, and here the error is much larger due to the

subsequent strong reflection. This method generally gives an approximation within 20 % accuracy, and the subsequent length refinement procedure reduces the error substantially.

3.4.2 Length Estimate Refinement: Cross-Correlation

The error of the initial length approximation is generally too large to be acceptable; thus, the estimation has to be refined during the node and TP type identifications (which are discussed in the next section). The refinement process involves two steps:

1. Computation of the cross-correlation between the windowed measurement and the model TDR responses over the RUI, and
2. Length adjustment using the cross-correlation lag $k_{\max}$ where the two responses are most similar.

A cross-correlation between two sequences provides a reference of how similar these sequences are in their shapes. The cross-correlation that we have applied includes both a normalizing and a centering operation to disregard energy level differences. In addition, the cross-correlation is only applied locally, over a window. The general mathematical expression for the windowed cross-correlation between two sequences x_n and z_n is

$$r_{xz}(k) = \sum_{n=n_r}^{n_r+N_w} \frac{(x_n - \mu_x)(z_{n+k} - \mu_z)}{\|x_n\|_2 \|z_{n+k}\|_2} \tag{3-9}$$

where k indicates the lag index and N_w is the window width. μ_x and μ_z are the means,

$$\mu_x = \frac{1}{b-a+1}\sum_{n=a}^{b} x_n \,, \tag{3-10}$$

while $\|x_{n-\tau}\|_2$ and $\|z_n\|_2$ are the respective 2-norms, of the windowed sequences, defined as

$$\|x_n\|_2 = \sqrt{\sum_{n=n_r}^{n_r+N_w} x_n^2} \,. \tag{3-11}$$

Both the mean and the 2-norm are computed exclusively over the cross-correlation window. Equation (3-9) guarantees that $r_{xz}(k)$ will always fall in the range between –1 and 1. Cross-correlation values of

1 and –1 indicate most correlated and most inversely correlated, respectively. Conversely, a cross-correlation value of zero suggests no correlation between the sequences.

In the fine-tuning of an estimated segment length, the cross-correlation is employed using the windowed TDR measurement and the partial model based on the most recently estimated segment length. The length is adjusted according to the lag index $k_{\max}$ where the maximum correlation occurs. For this method to work, the two windowed signals must have the same shape. This implies that the initial length estimate, which typically has an error of about ±20 %, must not cause reflection shape discrepancies between the measurement and the partial model. Instead, the difference between the two signals should be explained by the TOA offset and amplitude scaling. Furthermore, to enhance the RUI, the TDR response of the previous partial model is subtracted from both the measurement and the current partial model. The window width N_w is initially defined as the input pulse width. Ideally, the cross-correlation window size is based on the expected duration of the reflection. However, the dispersive nature of the TP causes the reflection width to be large . The conversion from $k_{\max}$ to the refined length estimate is obttained from

$$\hat{l}^{(new)} = \hat{l}^{(prev)} + \frac{\tilde{u}_g k_{\max}}{2 f_s} \tag{3-12}$$

where $\hat{l}^{(prev)}$ and $\hat{l}^{(new)}$ are the original and adjusted length estimates, respectively.

To demonstrate the refinement process, let us revisit the approximation of the first segment of the example loop with a GC as a continuation from the previous section's example (its actual and model TDR responses are shown in Figure 3-6). The initial guess for the length of the first segment — based on initial length estimation — was 175.75 m. We assume that the node type is GC, and the following segment is 26 AWG. The actual loop, the model after the first iteration, and the model with the length estimate and correct reflection node configuration are shown in Figure 3-11. Their corresponding TDR responses are illustrated in Figure 3-12. The objective is to adjust the initial length estimate (175.75 m) so that it is as close as possible to the actual length (150 m).

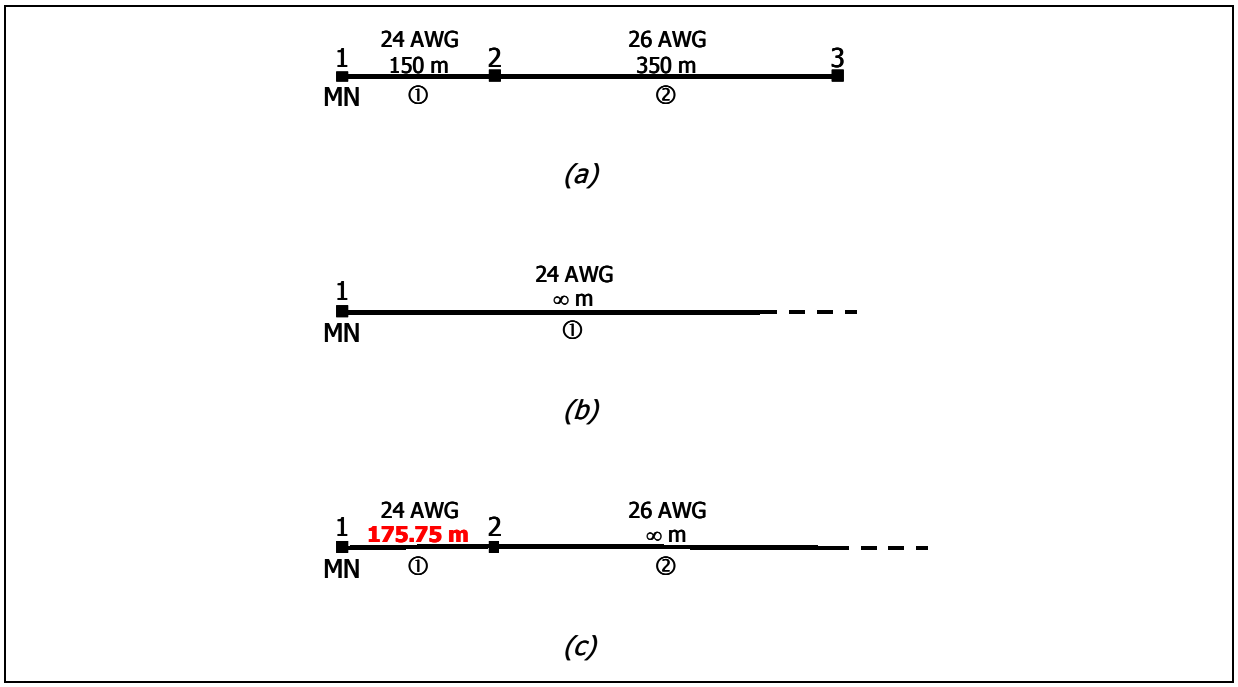

Figure 3-11: Actual structure of LUI (a) and model structure after 1st iteration (b) and after incorporation of estimated length (red) and subsequent structure (c). (MN — measurement node)

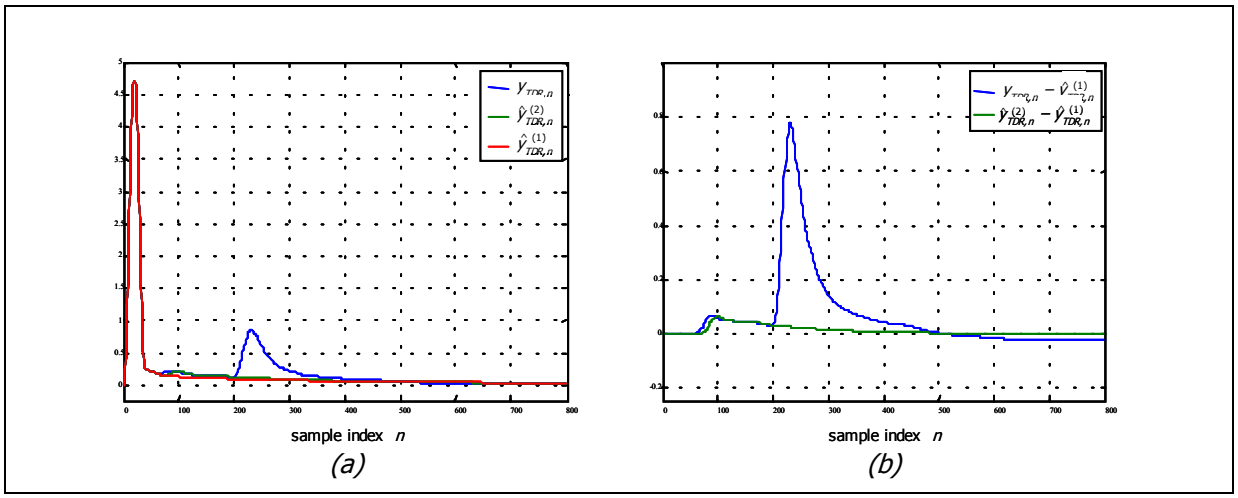

Figure 3-12: TDR responses of measured, model after 1st iteration, and model with length estimate (a); measured and model with length estimate after subtracting the 1st iteration model (b).

The first step in the refinement is to remove the TDR response based on the partial model obtained from the previous iteration, which is the first iteration in this case. The removal of the previous model response from both the measurements and the current model responses yields Figure 3-12(b). The windowed cross-correlation is computed with respect to these signals. The correlation

window with its lag origin at $n = n_r = 74$ is shown in Figure 3-13. The cross-correlation is computed by equation (3-9), while sliding the windowed model response across the measured response. The window offset from the origin is the lag index. The resulting cross-correlation plot is shown in Figure 3-14. The dashed red line in the figure indicates the peak of the cross-correlation curve and indicates $k_{\max} = -10$. Based on equation (3-12), the resulting adjustment yields –23.75 m and a refined length estimate of 150.287 m, which is much closer to the actual length of 150 m (< 1 % error).

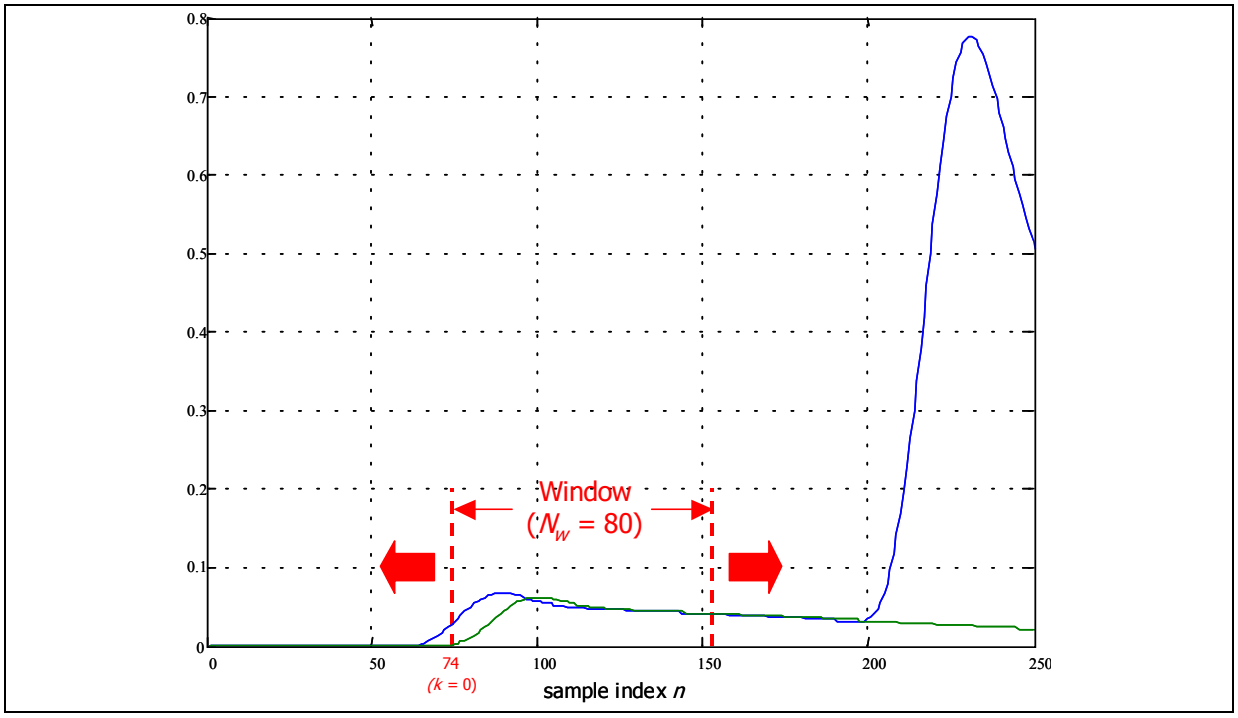

Figure 3-13: Correlation window for the refinement of the second iteration model in Figure 3-11(c).

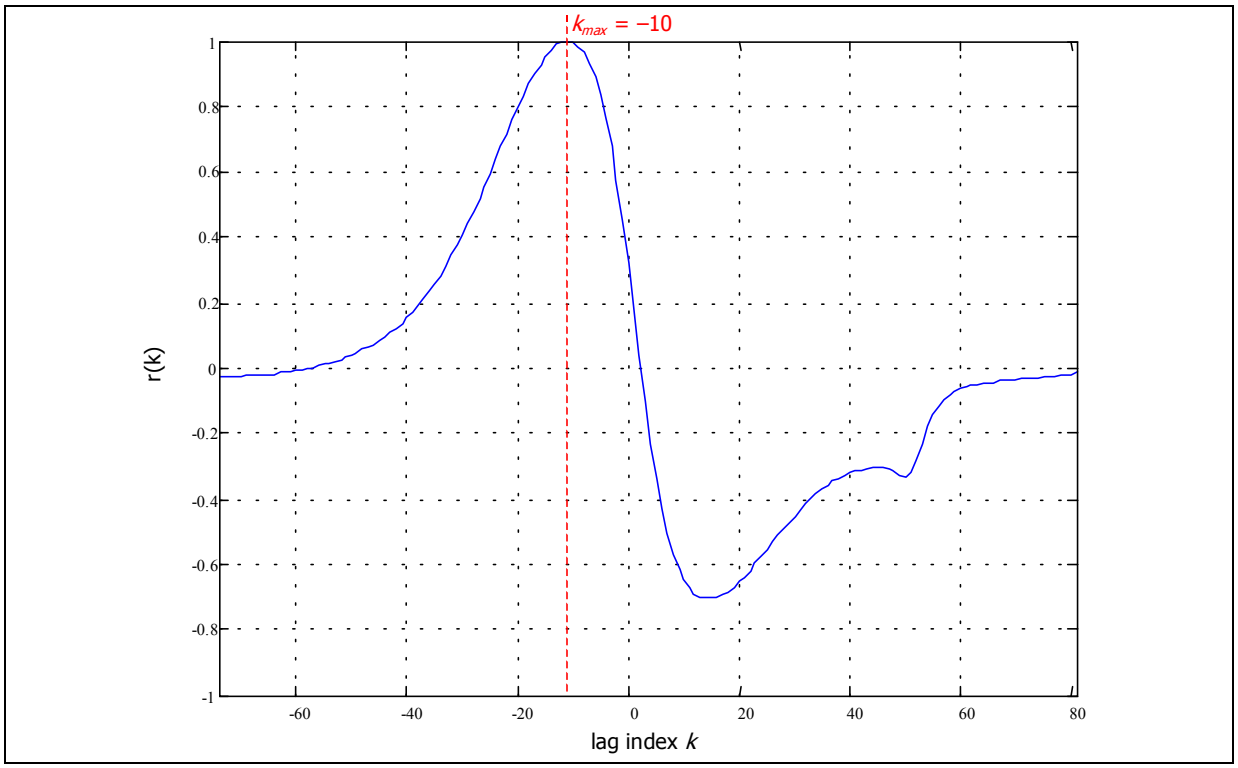

Figure 3-14: Cross-correlation of the TDR responses with the window defined in Figure 3-13.

As illustrated in the above example, this procedure is capable of finding the length with respectable accuracy. If desired, further accuracy may be obtained by interpolating the cross-correlation sequence. The actual estimation of the reflection node structure (which is assumed to be known in the above example) will be addressed in the next section, where the refinement routine is integrated with the candidate generation/selection process.

3.4.3 Model Candidate Generation and Best Candidate Selection

The node type (TP configuration at the reflection node) and line type of the TP connected to the reflection node (as well as the reflection node location, if multiple infinitely long segments exist) are identified through compilation of possible candidates and then selecting the best candidate. This section describes the necessary procedure for building the candidate pool composed of all possible node locations and configurations. In general, there are nine candidates for a node location with three node types and three TP types.

First, the potential location of the new node needs to be considered. As mentioned in the previous section, the new node can be placed on any of the existing infinitely long segments. The

exception is when the same line-type segment shares the same base node. In this case, only one of the two infinitely long segments needs to be considered.

Secondly, all possible node types (termination, GC, and BT) are modeled at each potential node location. They are illustrated in Figure 3-15 with a description of the segments attached to the node. Note that the estimated length and TP type of the segment that leads to the measurement node is already known. On the other hand, all of the segments that are newly added, in the GC and BT cases, are modeled as being infinitely long and having an unknown TP type.

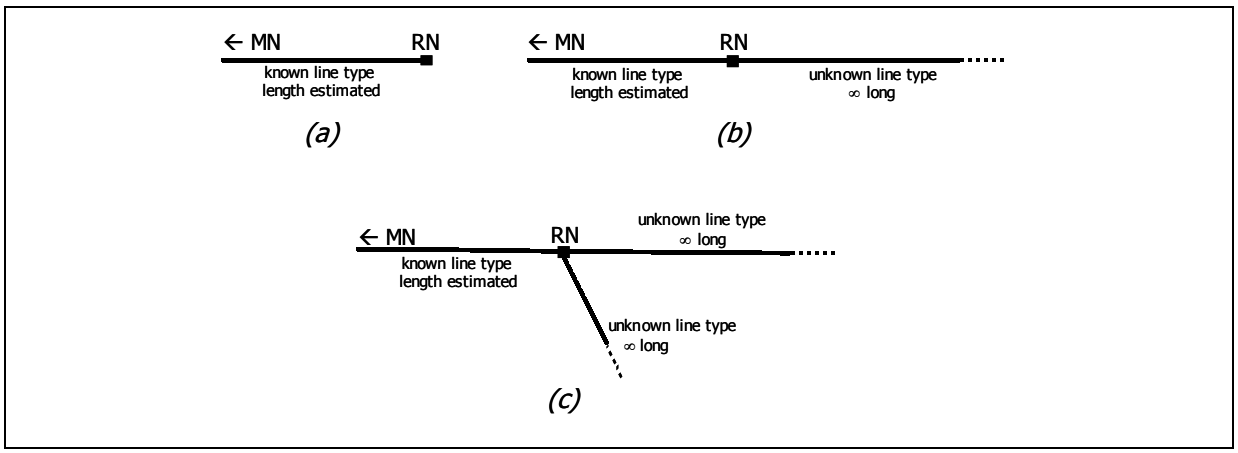

Figure 3-15: Possible node types—termination (a), gauge change (b), and bridged tap (c). (←MN—the location of the measurement node; RN—reflection node)

Lastly, these unknown TP types need to be identified through the generation of candidates for all cases. The possible combinations of line types (only 22, 24, and 26 AWG TP are being considered) are shown in Table 3-1. The left column shows the GC cases and the right column displays the BT cases. There are six BT cases instead of nine because the order of two unknown segments (*e.g.*, 22 AWG/ 24 AWG vs. 24 AWG / 22 AWG) is indistinguishable. Also, one of the GC candidates that matches with the known segment TP would not be considered since the unchanged TP, under ideal conditions, does not cause a reflection.

Table 3-1: Line type combination possibilities for one or two subsequent segment(s).

Node Type: GC — Figure 3-15(b) (1 unknown segment)	*Node Type*: BT — Figure 3-15(c) (2 unknown segments)
22 AWG	22 AWG / 22 AWG
24 AWG	22 AWG / 24 AWG
26 AWG	22 AWG / 26 AWG
	24 AWG / 24 AWG
	24 AWG / 26 AWG
	26 AWG / 26 AWG

Selection of the best candidate is obtained in two steps. First, the aforementioned length refinement procedure is applied to all of the candidates to improve the corresponding length estimates. Based on the cross-correlation, the inversely-correlated candidate is removed from consideration. A candidate is inversely-correlated if

$$\left|\min_{k}\left(r(k)\right)\right| > \left|\max_{k}\left(k\right)\right| \tag{3-13}$$

For each of the refined model's TDR responses, the weighted sum of squared errors (WSSE) is computed. The expression for the *j*-th candidate WSSE is equivalent to the last WCSSE value, or

$$WSSE_j = WCSSE_{j,N-1} = \sum_{n=0}^{N-1} w_n e_{j,n}^2 \,. \tag{3-14}$$

The same weighting function w_n is applied to the WSSE to de-emphasize the later reflections. The best candidate model j^* is simply the one that minimizes the $WSSE_j$ criterion.

To demonstrate the candidate generation/selection process, the GC example is once again revisited. Recall that we assumed the correct node configuration to be already known in the previous example, when dealing with length refinement. This example generates all of the candidates and shows the correct candidate model to be selected indeed. With the result of the first iteration shown in Figure 3-11(b) and the initial length estimation of 175.75 m, the 9 possible candidates are illustrated in Figure 3-16. All candidates' TDR responses are computed and plotted with the LUI TDR response in Figure 3-17 (from visual inspection, it is apparent that the 26 AWG GC is the best fit of all candidates). Furthermore, the corresponding cross-correlations between each candidate and the LUI responses are shown in Figure 3-18. As can be readily verified from looking at Figure 3-17, only the termination and GC–26 AWG cases are positively correlated with the LUI response. The length

refinement and WSSE of the two remaining candidates are shown in Table 3-2. The correct candidate, GC—26 AWG, is selected by WSSE criterion.

Table 3-2: Final Candidates for GC example. GC: 26 AWG selected.

Candidate	Refined Length	WSSE
Termination	176.4120 m	1.528×10^{-2}
GC: 26 AWG	150.2870 m	3.235×10^{-4}

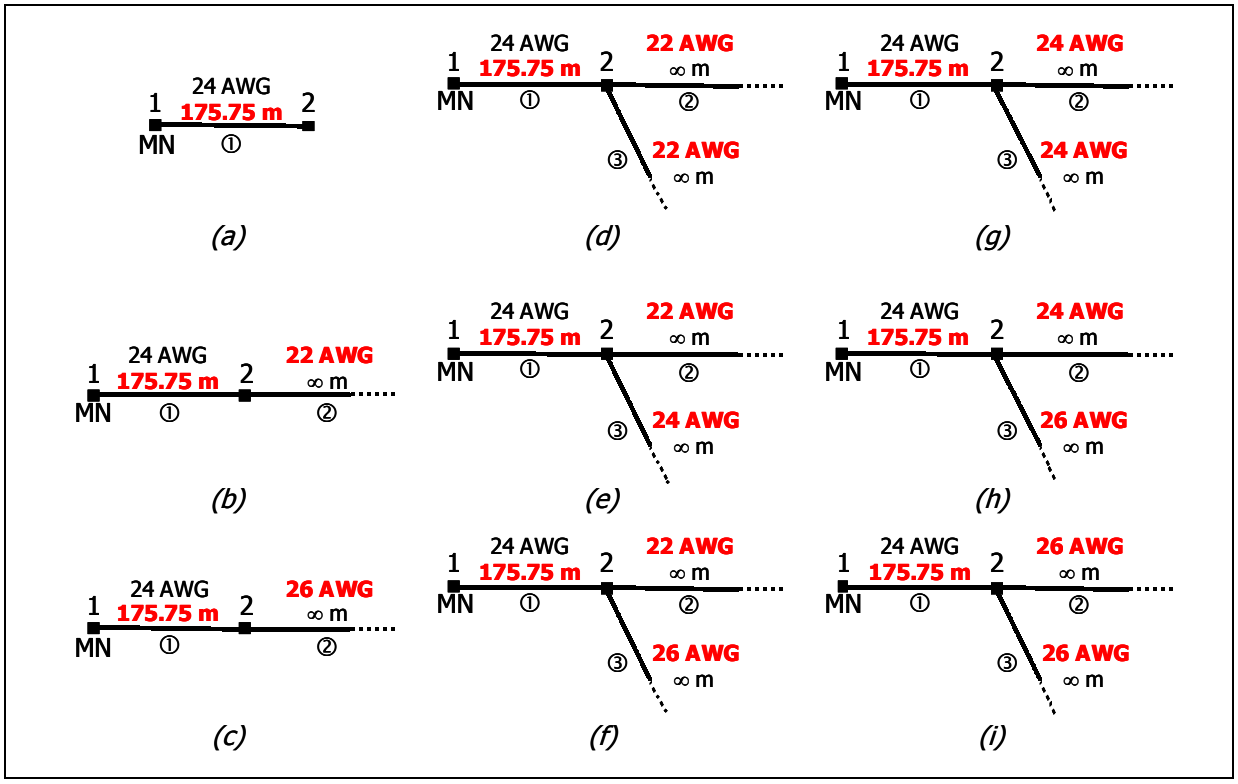

Figure 3-16: All potential node configurations for the identification of the GC node.

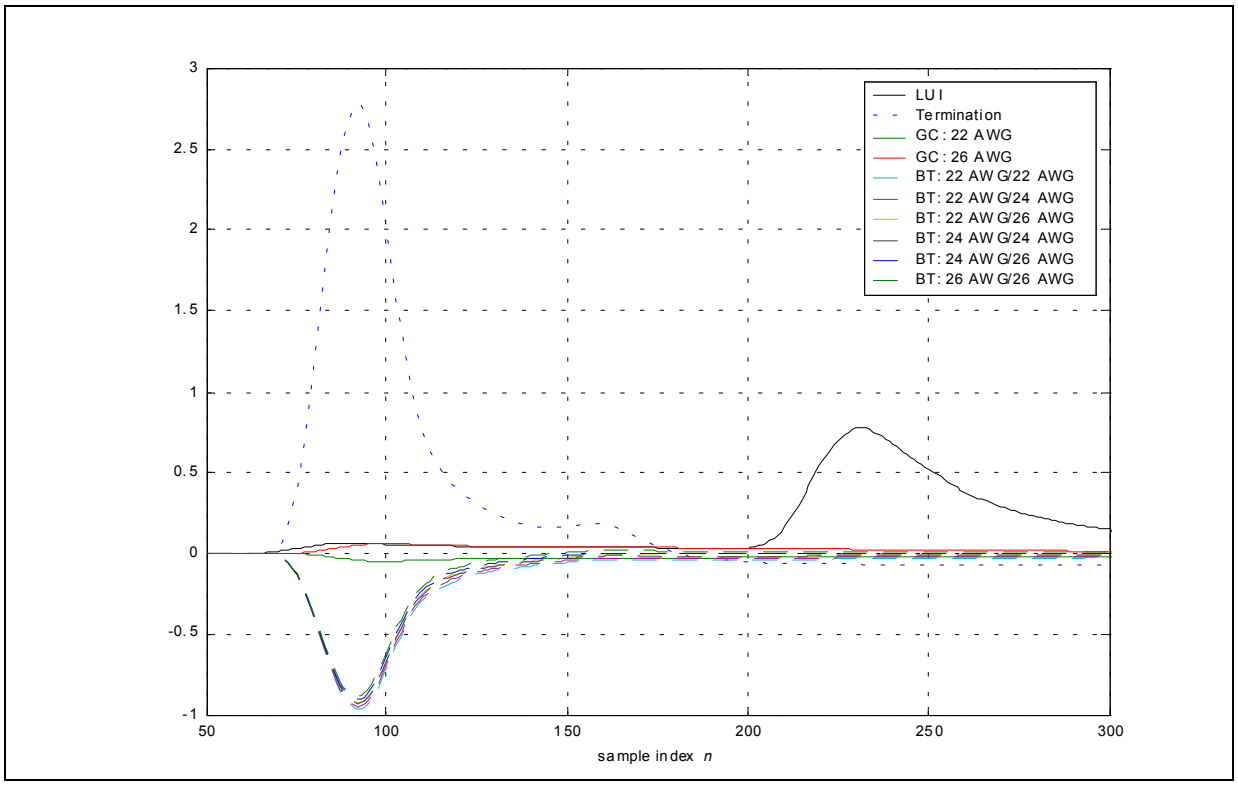

Figure 3-17: TDR responses of all candidates and the LUI after subtraction of the first iteration model.

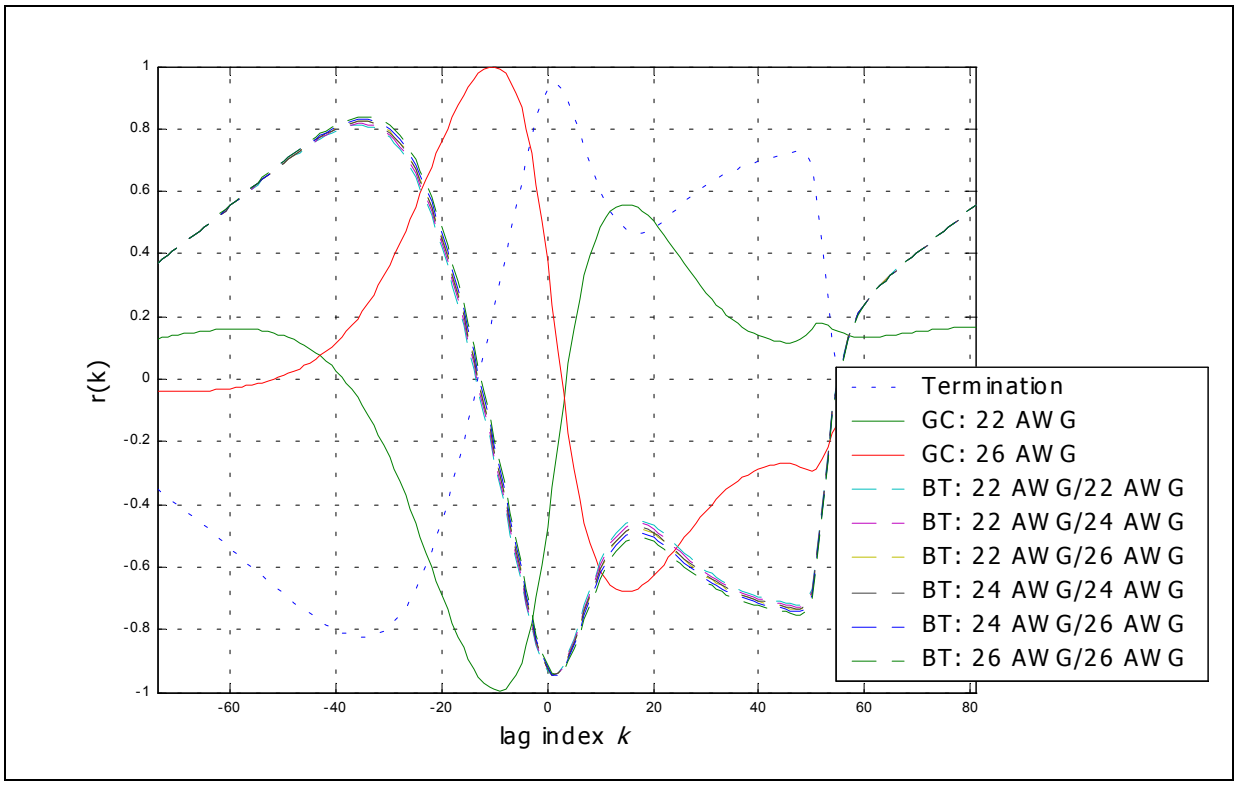

Figure 3-18: Cross-correlation between the measurement and each candidate.

3.5 Problem with Heavily Overlapping Reflections

While this time-domain identification procedure functions correctly with segment length estimation within 3 m with respect to the actual, the procedure starts to fall apart when more than two reflections overlap with each other obscuring the full shape of the reflection. This trend becomes critical to estimate the loop structure after a long initial segment or the far-end network because of the twisted-pair's dispersive behavior. With our objective of the local loop identification from the central office (CO) end — with connection to the main cable, typically long — this inability of the algorithm is highly undesirable. To demonstrate this shortcoming of the time-domain loop identification process, the identification of the CSA #1 test loop (see Appendix A for its structure) measured from Node 1 is documented in the remaining of the section.

The TDR response is generated with the 10-V 1-μs raised-cosine pulse, shown in Figure 2-7, and sampled at 40 MHz. The TDR response is stored for 2^{15} samples. The measurement equipment input impedance is assumed to be a purely resistive 120 Ω. The first 1,500 samples of the TDR response measured from Node 1 are shown in Figure 3-19. The first iteration readily detects the 26 AWG single segment with ease as shown in Figure 3-20.

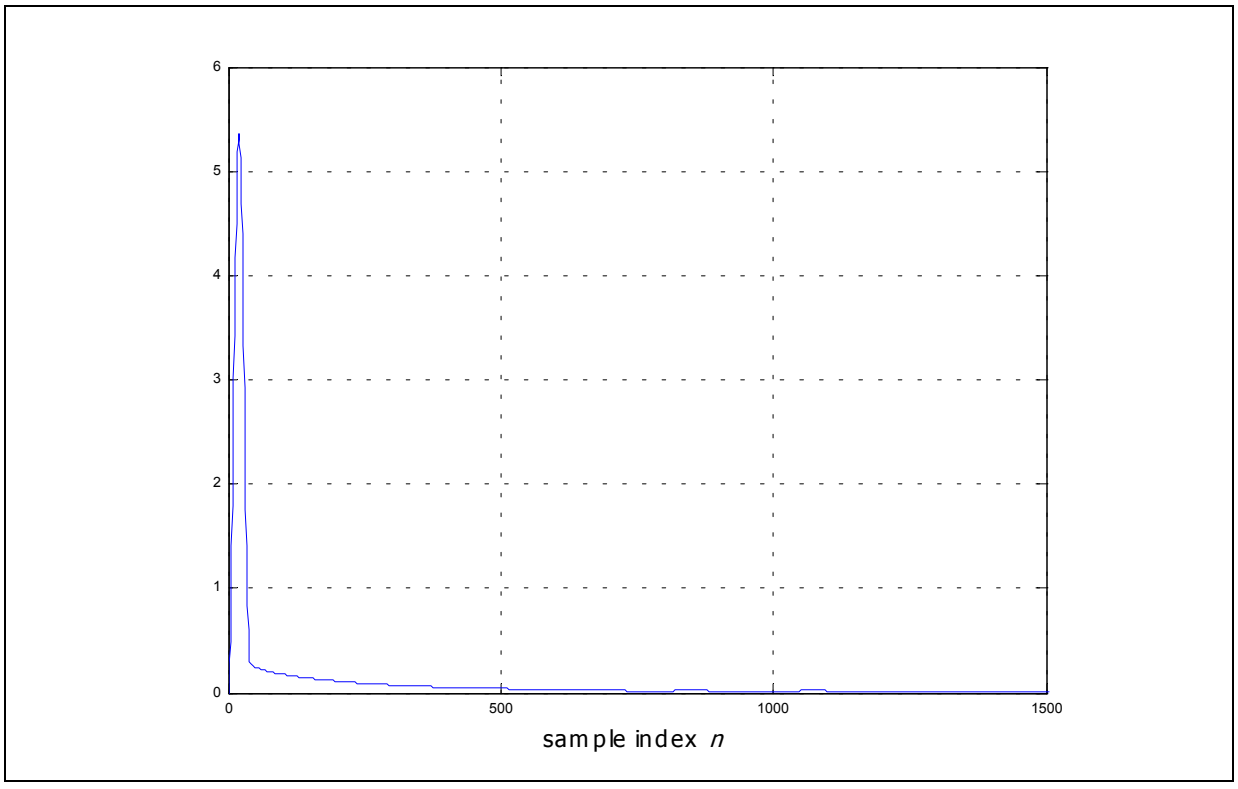

Figure 3-19: CSA #1 TDR response measured from Node 1.

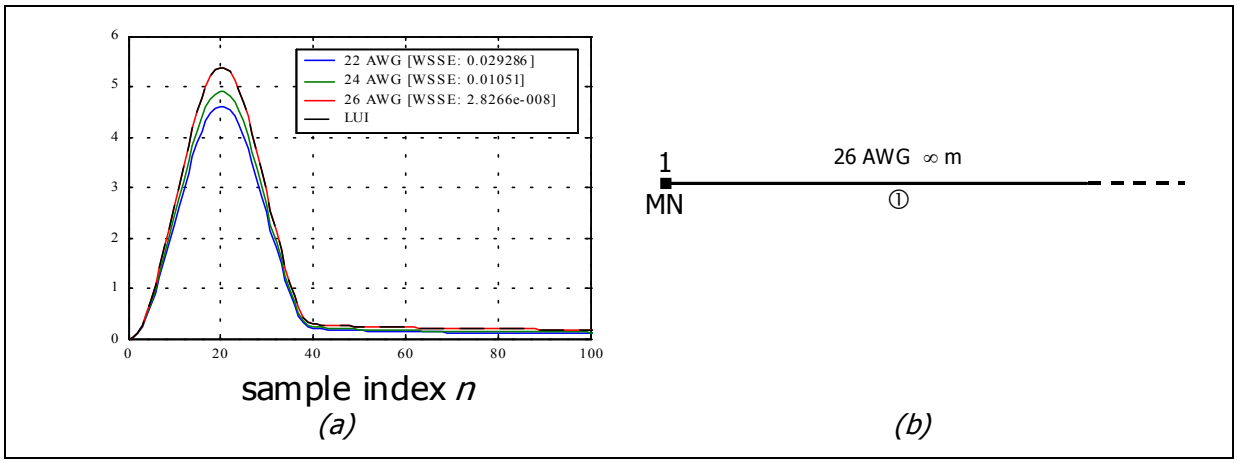

Figure 3-20: CSA #1 Node 1 First Iteration — candidate TDR response fit to the LUI (a) and the resulting partial model (b). WSSE for each candidate shown in the legend (a).

However, the residual after the first iteration, as shown Figure 3-21 is a linear combination of at least three major reflections as illustrated in Figure 3-22. To proceed with the next iteration cycle, the first remaining reflection (blue reflection in Figure 3-22) needs to be separated resulting in a BT node 5,900 ft (~1,800 m) from Node 1 with two 26-AWG TP segments following the node. Under the assumption of known 5,900 ft. segment length, the candidate TDR responses are shown with that of the LUI in Figure 3-23. The LUI response follows the correct candidate — BT node with two 26-AWG segments — until the arrival of the next reflection ($n \approx 780$). The next reflection arrives well before the RUI subdues, and the subsequent reflections — heavily dispersed — cause greater mismatch between the LUI and the correct candidate responses. The corresponding WSSEs, tabulated in Table 3-3, indicate that the minimum WSSE candidate is the GC followed by a 24-AWG TP — an obvious misidentification — despite that the weighting function penalizes later reflections.

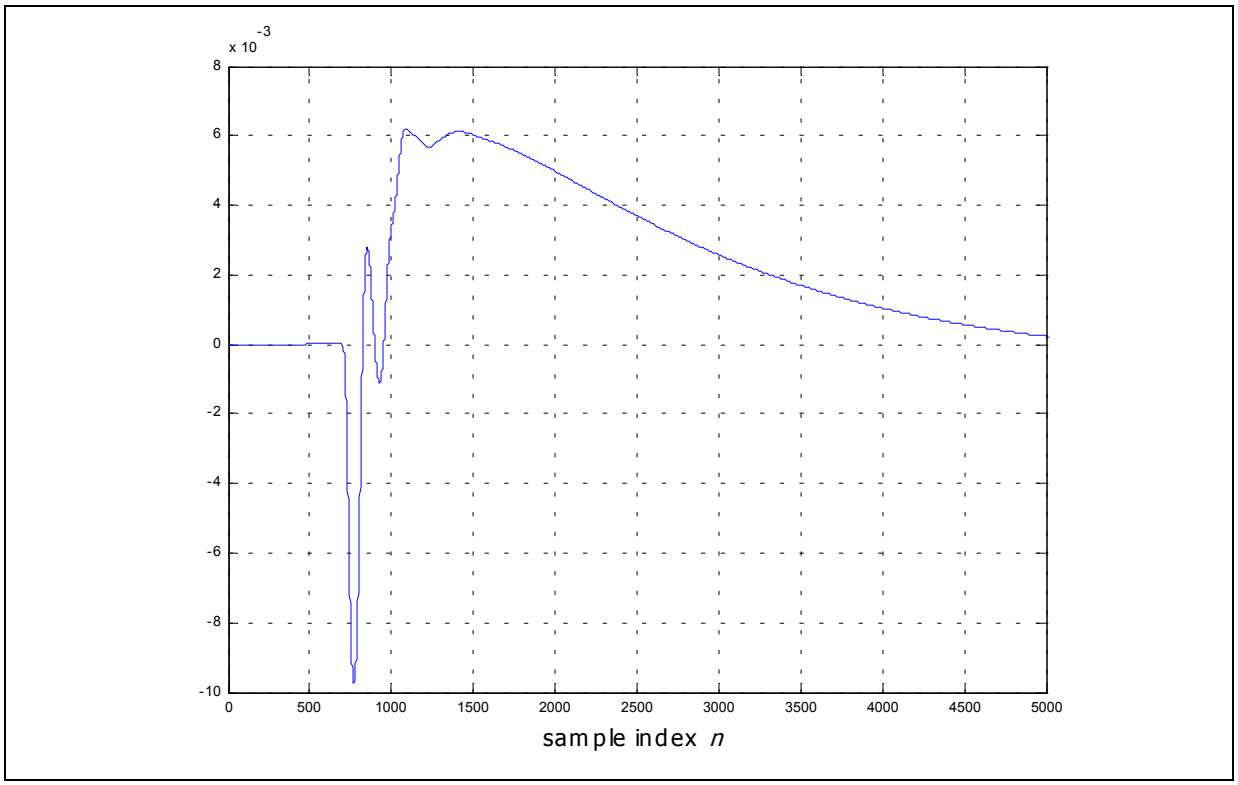

Figure 3-21: Residual after the first iteration for CSA #1 measured from Node 1.

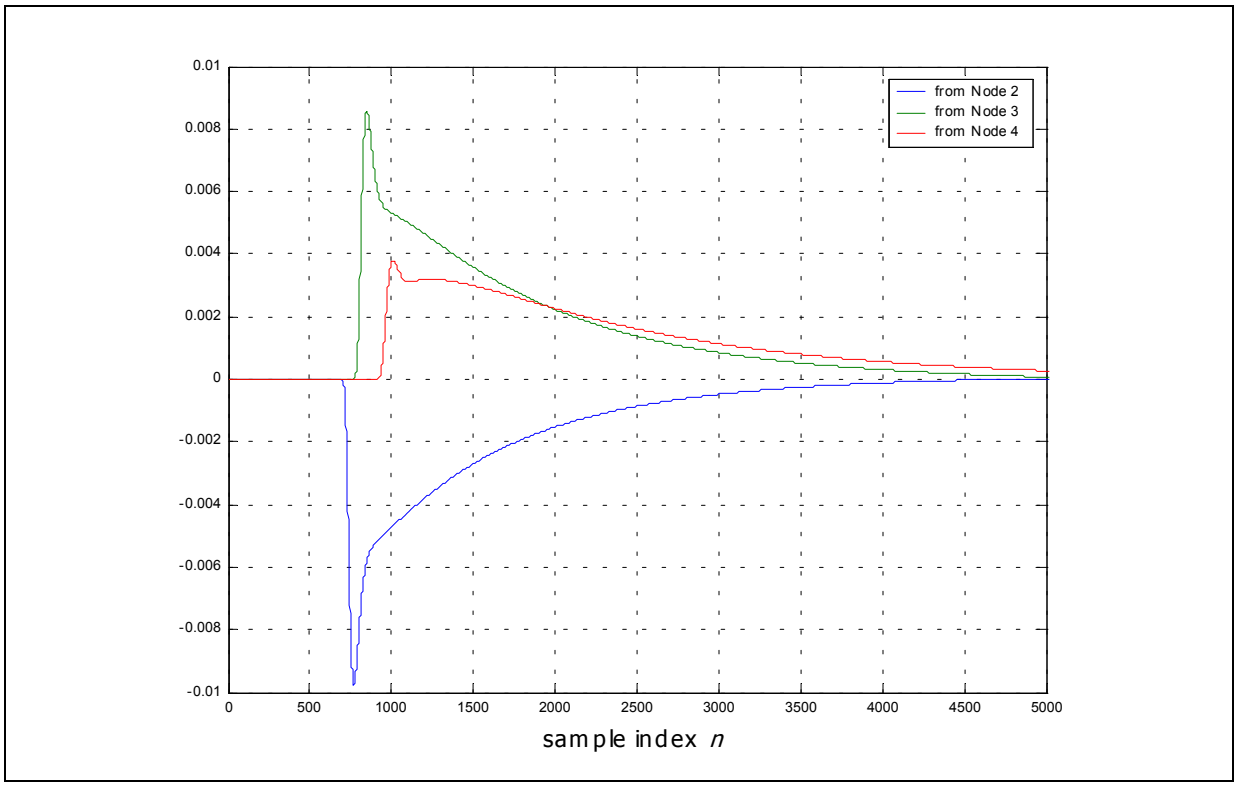

Figure 3-22: Initial reflections from remaining nodes superimposed in the residual in Figure 3-21.

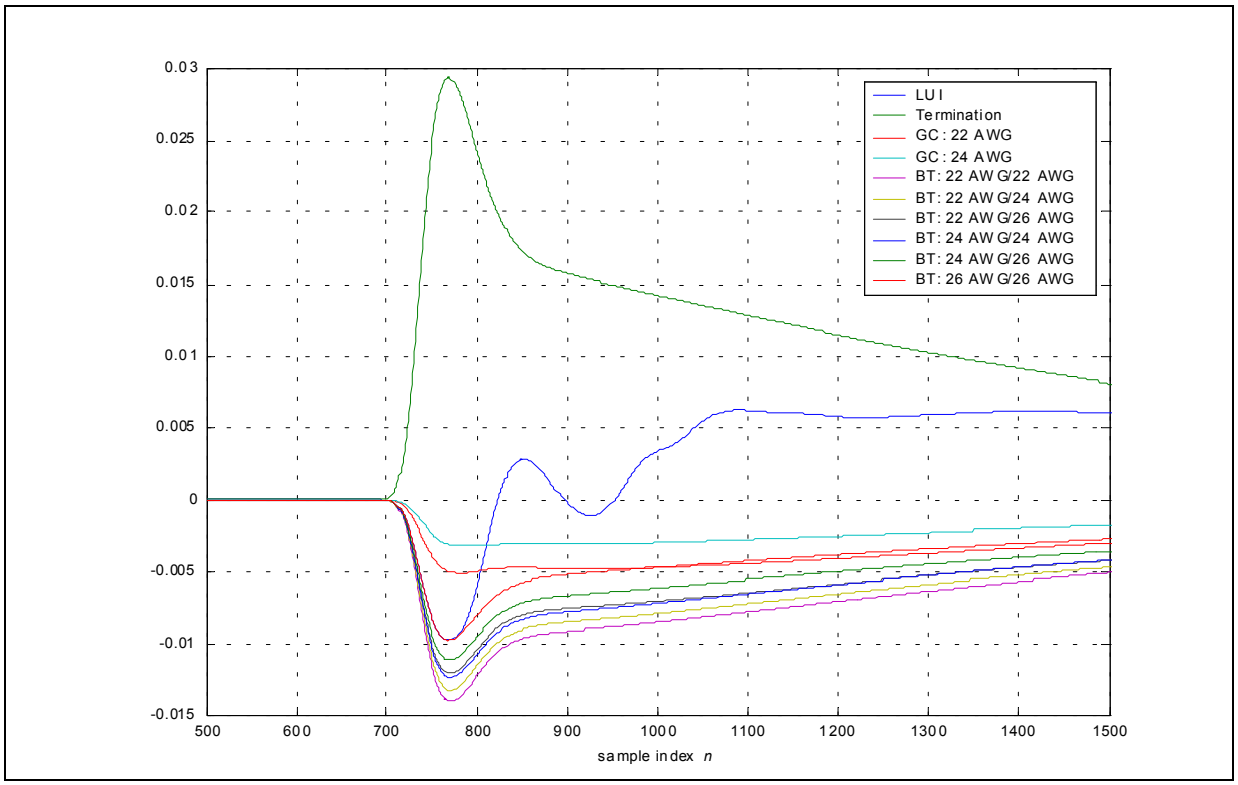

Figure 3-23: LUI and Candidate TDR responses (removed 1st reflection) in 2nd Iteration for CSA #1 measured from Node 1. (5,900 ft. assumed known)

Table 3-3: WSSE for candidates in Figure 3-25. Minimum WSSE highlighted.

Candidate	WSSE	Candidate	WSSE
Termination	2.1901×10^{-7}	BT: 22 AWG / 26 AWG	8.3192×10^{-8}
GC: 22 AWG	5.7065×10^{-8}	BT: 24 AWG / 24 AWG	8.4736×10^{-8}
GC: 24 AWG	4.2494×10^{-8}	BT: 24 AWG / 26 AWG	7.0895×10^{-8}
BT: 22 AWG / 22 AWG	1.0478×10^{-7}	BT: 26 AWG / 26 AWG	5.5039×10^{-8}
BT: 22 AWG / 24 AWG	9.5384×10^{-8}		

3.6 Summary

This chapter describes an approach to subscriber loop identification using TDR measurements. An iterative procedure, which can be reliably applied for limited loop structures, is proposed which exploits the information embedded in the individual reflections of the TDR response. Each reflection returns from a particular node in the loop and incorporates sufficient information to determine the related loop parameters. One reflection is processed per iteration, each time revealing a new node of the subscriber loop and updating the partial loop model accordingly.

The iteration consists of two distinctive stages. The first stage is the detection of the earliest unprocessed reflection, and is followed by the loop parameter estimation stage based on the detected reflection. The WCSSE criterion is employed for the detection stage, while the parameter estimation stage utilizes several techniques such as cross-correlation, WSSE, and systematic model candidate generation.

The problem arises when the reflections are heavily overlapped. This occurs for an LUI that has a long segment followed by short segments or a far-end network. The reflections returning from short segments at the far end are inevitably heavily overlapping, due to the dispersive nature of the TPs. This overlapping causes a great deal of "confusion" in the identification procedure. Thus, the procedure fails and is unable to identify the short segment network at the far end of the loop. In Chapter 4, this problem will be viewed as a type of time delay estimation problem where the time-of-arrival (TOA) of known superimposed signals is to be estimated.